Catalysis Today 335 (2019) 144–150

Contents lists available at ScienceDirect

Catalysis Today

journal homepage: www.elsevier.com/locate/cattod

Protocatechuic acid promoted catalytic degradation of rhodamine B with Fe@Fe_2O_3 core-shell nanowires by molecular oxygen activation mechanism

Yaxin Qin[a], Guiying Li[a], Lizhi Zhang[b,*], Taicheng An[a,*]

[a] Guangzhou Key Laboratory of Environmental Catalysis and Pollution Control, School of Environmental Science and Engineering, Institute of Environmental Health and Pollution Control, Guangdong University of Technology, Guangzhou 510006, China

[b] Key Laboratory of Pesticide & Chemical Biology of Ministry of Education, Institute of Environmental Chemistry, College of Chemistry, Central China Normal University, Wuhan 430079, China

ARTICLE INFO

Keywords:
Protocatechuic acid addition
Fe@Fe_2O_3 core-shell nanowires
Molecular oxygen activation
Complexing and reduction abilities
Fe(III)/Fe(II) cycle

ABSTRACT

The addition of ligands into the system of zero valent iron is an effective method to promote the yields of pollutants oxidant but may lead to the unfavorable environmental consequences. In this study, the addition effects of protocatechuic acid (PCA), a kind of complexing and reducing agent widely existed in many plants, on the molecular oxygen activation and the subsequent aerobic rhodamine B degradation by Fe@Fe_2O_3 core-shell nanowires were investigated. Results indicated that the degradation efficiency of rhodamine B increased from less than 6% to 92.4% within 120 min with the PCA addition in the system of Fe@Fe_2O_3 core-shell nanowires. This addition of PCA not only promote the molecular oxygen activation efficiencies induced by Fe@Fe_2O_3 core-shell nanowires, but also accelerate the Fe(III)/Fe(II) cycle to guarantee enough soluble Fe(II) for subsequent efficient Fenton reaction. Moreover, PCA can also defer the oxidation of Fe@Fe_2O_3 core-shell nanowires for its reduction ability. X-ray photoelectron spectroscopy and X-ray diffraction characterization revealed that there were no significant changes of the compositions of Fe@Fe_2O_3 core-shell nanowires before and after reactions in the system with PCA addition. Meanwhile, only slightly decrease of the rhodamine B degradation efficiency was observed after 4 cycles in the system of Fe@Fe_2O_3 core-shell nanowires and PCA. This study not only clarify the effects of PCA on the molecular oxygen activation by nanoscale zero-valent iron, but also sheds new insight into the possible roles of widely existed phenolic acids in the transformation of organic contaminants with nanoscale zero-valent iron in natural aquatic environment.

1. Introduction

Current fresh water shortages induced by the increasing world population and rapidly evolving industries, impose great pressures on the water purification and recycling. So, much attention has been focused on advanced oxidation processes (AOPs) which have the capability to exploit nonselective active species (such as hydroxyl radical) and mineralize the contaminants to CO_2 and H_2O [1–3]. As one of the most earth-abundant metals, zero valent iron (ZVI) has been recognized as a very promising material for water remediation due to its cost-effectiveness, high reactivity, and environmental friendliness [4–7]. Nowadays, ZVI has been widely used as a reductant to reduce heavy metal ions (*e.g.* Cr(VI), and Pb(II)) [8–11] and chlorinated and nitro-substituted organic pollutants [12–15] through the direct electron transfer from ZVI to the contaminants. It is also a heterogeneous catalyst to decompose H_2O_2 [16–18], O_3 [19], and persulfate [20–23] to generate $^{\cdot}OH$ or $SO_4^{\cdot -}$ for organics degradation. Moreover, recent studies indicated that ZVI could react with molecular oxygen to produce reactive species (RS), including $^{\cdot}OH$, H_2O_2, $O_2^{\cdot -}$ and ferryl ion (Fe^{IV}), which are able to oxidize or even mineralize organic compounds [24–26]. Therefore, the molecular oxygen activation with ZVI is highly desirable for the environmental remediation in view of environmental friendliness [27–29]. Unfortunately, the practical application of ZVI/O_2 system is restricted by the low yields of RS, though the generation of RS through the reaction of molecular oxygen and ZVI has been reported for many years. It has been demonstrated that only 7% of ZVI could react with molecular oxygen to produce RS at neutral pH in ZVI/O_2 system [30].

Enormous efforts have been devoted to improve the utilization efficiency of ZVI by adding ligands, such as oxalate, ethylenediaminetetraacetic acid (EDTA), and so on [31–35]. Sedlak et al. has reported that the yields of oxidants almost reached their theoretical maxima near

* Corresponding authors.
E-mail addresses: zhanglz@mail.ccnu.edu.cn (L. Zhang), antc99@gdut.edu.cn (T. An).

https://doi.org/10.1016/j.cattod.2018.10.058
Received 4 September 2018; Received in revised form 18 October 2018; Accepted 24 October 2018
Available online 08 November 2018
0920-5861/

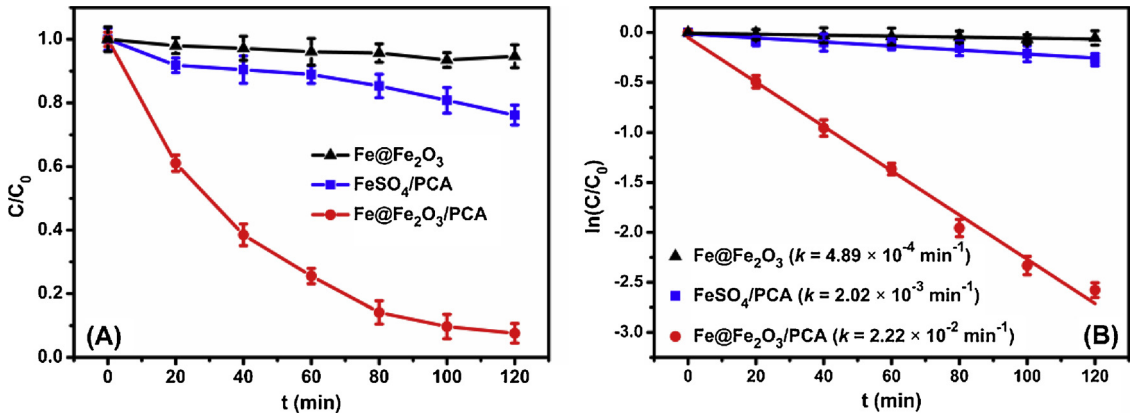

Fig. 1. (A) Time profiles of the aerobic RhB degradation in different systems. (B) Plots of $\ln(C/C_0)$ *versus* time for the aerobic RhB degradation in different systems. The initial concentrations of RhB, $Fe@Fe_2O_3$, $FeSO_4$, and PCA were 5 mg L^{-1}, 4.5, 4.5, and 0.5 mmol L^{-1}, respectively.

neutral pH in the presence of oxalate, nitrilotriacetic acid (NTA), or ethylenediaminetetraacetic acid (EDTA) [36]. Our previous studies also reported that the degradation efficiency of 4-chlorophenol increased from 29.8% to 92.5% and 94.1% within 2 h with the addition of diethylenetriamine pentaacetate (DTPA) and EDTA, respectively [37]. Although the addition of organic ligands could enhance the RS generation efficiency, they may cause some undesirable environmental consequences due to their poor biodegradability and superior heavy metal chelating ability. Moreover, the presence of ligands may also accelerate the oxidation of ZVI, and thus resulting in the fast exhaustion of Fe^0 and the consequent decrease of organics degradation efficiencies. However, the effects of ligands on the activity and reusability of ZVI have received only little attention.

In this study, $Fe@Fe_2O_3$ core-shell nanowires, a special kind of modified ZVI was developed and used to systematically investigate the effects of PCA, a typical phenolic acid widely existed in natural environment, on the molecular oxygen activation and the subsequent degradation of rhodamine B (RhB). Meanwhile, EDTA, which is one of the most widely used complexing agent, was also used as a control to clarify the roles of PCA on the activity and reusability of $Fe@Fe_2O_3$ core-shell nanowires. The purpose of this study aims to deeply understand the interaction mechanisms of PCA with $Fe@Fe_2O_3$ core-shell nanowires and provide new insights into the roles of ligands in the molecular oxygen activation process with ZVI.

2. Experimental section

2.1. Chemicals and materials

$NaBH_4$ (96%), $FeCl_3{\cdot}6H_2O$ (AR), protocatechuic acid (PCA, AR), rhodamine B (RhB, AR), ethylenediaminetetraacetic acid (EDTA, AR), NaOH (AR), benzoic acid (AR), p-hydroxybenzoic acid (AR) and 1, 10-phenanthroline (AR), commercial iron powder (ZVI) were purchased from Sinopharm Chemical Reagent Co., Ltd. China. Superoxide dismutase (SOD), and catalase (CAT) were purchased from Sigma-Aldrich. All of these chemicals were used as received without further purification. De-ionized water was used in all experiments. $Fe@Fe_2O_3$ core-shell nanowires were prepared according to the same method described in our previous work [38]. Single Fe (T-ZVI) was obtained by washing ZVI with 0.1 mol L^{-1} H_2SO_4 within 5 min to remove the passive oxide layer.

2.2. Aerobic degradation of RhB

In a typical catalytic experiment, $Fe@Fe_2O_3$ core-shell nanowires (0.01 g, the molecular weight of the nanowires was assumed as 56) were dispersed into 40 mL of 5 mg L^{-1} RhB aqueous solution in the absence and presence of PCA or EDTA (0.5 mmol L^{-1}) without pH adjustment. For the comparison, the same number of moles of Fe^{II} was added instead of $Fe@Fe_2O_3$ core-shell nanowires. All experiments were carried out at room temperature (25 ± 5 °C) in 50 mL glass conical beaker. Air was supplied through an air pump to keep the air saturated and improve the contact between catalyst and the solution. At an interval of 20 min, a 3 mL aliquot of the solution was collected and filtered immediately through a 0.22 μm nylon syringe filter for UV–vis spectrometer analysis.

2.3. Analytical methods

X-ray diffraction (XRD) patterns were measured on a Bruker D8 Advance X-ray diffractometer with Cu Ka radiation. Scanning electron microscopy (SEM) images were performed on a LEO 1450 V P scanning electron microscope. X-ray photoemission spectroscopy experiments performed on a Kratos ASIS-HS X-ray photoelectron spectroscope equipped with a standard and monochromatic source (Al KR) operated at 150 W (15 kV, 10 mA).

The concentration of RhB was analyzed using a UV–vis spectrophotometer at its maximum absorption wavelength of 554 nm, and the concentration of iron ions was monitored by a modified method using 1, 10-phenanthroline with a UV–vis spectrophotometer (UV-2550, Shimadzu, Japan). The total organic carbon (TOC) content was determined using a Shimadzu TOC-V CPH analyzer. Benzoic acid was used as the probe for detection of hydroxyl radicals, and p-hydroxybenzoic acid (p-HBA), one of the major oxidation products was quantified by high performance liquid chromatography (HPLC, Agilent TC-C18 reverse phase column). The injection volume was set at 10 μL and the mixture of water and acetonitrile (60/40, v/v) was used as the mobile phase with a flow rate of 1.0 mL min^{-1}, and the detection wavelength was set at 225 nm. The degradation intermediates of RhB were identified by GC–MS (Thermo Fisher Scientific, Trace 1300 equipped with ISQ) with a DB-5 column (size 30 m × 0.25 mm).

3. Results and discussion

The degradation kinetic curves of RhB in different systems are shown in Fig. 1A. It was found that only 5.3% of RhB could be removed in the presence of $Fe@Fe_2O_3$ core-shell nanowires within 120 min, suggesting the low efficiency of molecular oxygen activation. With the addition of PCA, the degradation efficiency of RhB reached 92.4%, indicating that PCA could effectively enhance aerobic RhB degradation with $Fe@Fe_2O_3$ core-shell nanowires. The kinetic processes of RhB degradation fits well with pseudo first-order kinetics model and the calculated degradation rates were shown in Fig. 1B. The aerobic RhB degradation rate constant was obtained as 2.22×10^{-2} min^{-1} in the

Fe@Fe_2O_3/PCA system, which was about 40 times that in the Fe@Fe_2O_3 system (4.89×10^{-4} min^{-1}). Meanwhile, methyl orange (MO) and methylene blue (MB) was used as the typical representative of acidic and basic dye to clarify the selectivity of this system. The results indicated that 81.7% and 89.8% of MO and MB was degraded within 60 min (Fig. S1 in the Supporting information), indicating this system was also effective for other dye molecules. For comparison, the anaerobic RhB degradation in the Fe@Fe_2O_3/PCA system was also examined. The removal of oxygen by bubbling high-purity Ar completely inhibited the degradation of RhB (Fig. S2 in the Supporting information), which can not only reveal the necessity of oxygen during the RhB degradation, but also rule out the direct RhB reduction by Fe@Fe_2O_3 core-shell nanowires. One previous studies have demonstrated that ferrous complexes (such as Ferrous-tetrapolyphosphate complex) can also react with molecular oxygen to produce reactive species [39]. So, Fe@Fe_2O_3 core-shell nanowires were replaced by Fe(II) at similar concentration to clarify the roles of Fe(II) and PCA in the aerobic RhB degradation, although PCA can only form complexes with Fe(III). The results showed that 23.8% of RhB was degraded in the Fe(II)/PCA system (Fig. 1), indicating the contributions of Fe(II) and PCA in the RhB degradation. To further clarify the role of Fe core and Fe_2O_3 shell, we compared the degradation efficiencies of RhB in the system with ZVI and Fe_2O_3 and found that both ZVI and Fe_2O_3 could not effectively degrade RhB (Fig. S3 in the Supporting information). When H_2SO_4 (0.1 mol L^{-1}) was used to remove the iron oxide of ZVI, the degradation efficiency of RhB reached 81.7% within 120 min. This was because the surface of ZVI was easy to be oxidized and form a passive oxide layer, which would inhibit the molecular oxygen activation process.

Then, the concentration changes of dissolved ferrous and total iron ions were systemically compared in the Fe@Fe_2O_3 and Fe@Fe_2O_3/PCA systems. The results shown in Fig. 2 confirmed that the concentrations of dissolved ferrous ions and total iron ions in the presence of PCA are significantly higher than that in the absence of PCA, indicating that PCA could promote the continuous release of iron ions. The concentration of dissolved ferrous ions and total iron ions increased rapidly to the maximum value within first 40 min, and then decreased to 0 mmol L^{-1} after 120 min, which might be caused by the degradation of PCA. Meanwhile, the results also indicated that the concentration of ferrous ions just slightly lower than that of total iron ions, further conforming the pronounced reductive effect of PCA on the Fe(III)/Fe(II) cycle. Our previous work has demonstrated that dissolved ferrous ions could enhance single-electron reduction molecular oxygen activation by providing more surface bound ferrous ions onto the iron oxide shell [40]. So, the high concentration of ferrous ions may also affect the yields of RS, and thus affect the degradation of RhB.

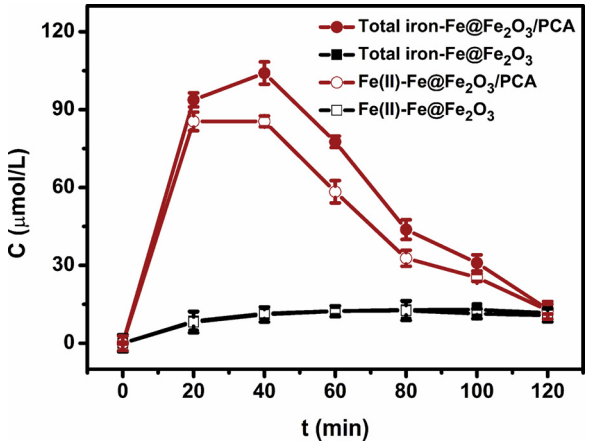

Fig. 2. Variation of total iron ions and ferrous ions concentrations in different systems during the aerobic RhB degradation. Initial concentrations of Fe@Fe_2O_3 and PCA were 4.5 and 0.5 mmol L^{-1}, respectively.

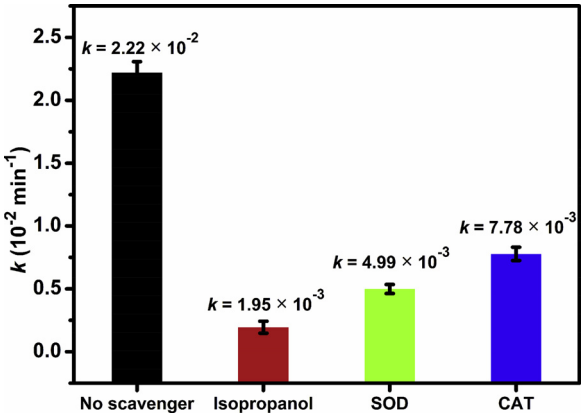

Fig. 3. The aerobic RhB degradation rate constants in the Fe@Fe_2O_3/PCA system with adding different scavengers (isopropanol for $^{\cdot}OH$, SOD for $^{\cdot}O^{2-}$, CAT for H_2O_2). The initial concentrations of RhB, Fe@Fe_2O_3, and PCA were 5 mg L^{-1}, 4.5, and 0.5 mmol L^{-1}, respectively.

Obviously, the presence of PCA not only act as a complexing agent, but also enhance the concentration of ferrous ions to promote the molecular oxygen activation process of Fe@Fe_2O_3 core-shell nanowires. A series of experiments were then carried out to clarify the generation of RS in the Fe@Fe_2O_3/PCA system by adding different kinds of scavengers (isopropanol for $^{\cdot}OH$, SOD for $^{\cdot}O_2^-$ and CAT for H_2O_2). As shown in Fig. 3, the aerobic RhB degradation was largely depressed by the addition of isopropanol, revealing the major role of $^{\cdot}OH$ in the degradation of RhB. The presence of SOD and CAT also inhibited the degradation of RhB, suggesting that $^{\cdot}O_2^-$ and H_2O_2 were also involved in the Fe@Fe_2O_3/PCA system. As well-known, $^{\cdot}O_2^-$ can only be generated though the single-electron reduction of molecular oxygen, and H_2O_2 can be produced through either the sequential single-electron transfer ($O_2 \rightarrow {}^{\cdot}O_2^- \rightarrow H_2O_2$) or the two-electron transfer ($O_2 \rightarrow H_2O_2$) routes. To further understand the activation mechanism of molecular oxygen catalyzed by Fe@Fe_2O_3 and PCA, the inhibitory efficiency (η) of SOD and CAT were calculated through Eq. (1) [41].

$$\eta\% = \left[\frac{k_0 - k_t}{k_0}\right] \times 100\% \quad (1)$$

Where k_0 and k_t were the apparent degradation constants in the absence or presence of scavenger, respectively. It was assumed that RS could be completely trapped by excess scavengers. The results indicated that 77.5% and 64.9% of RhB degradation depression caused by the addition of SOD and CAT. Since the addition of SOD would induce a dismutation reaction to consume two $^{\cdot}O_2^-$ and generate a H_2O_2 (Eq. (2)). The yield of H_2O_2 was only 50% of that *via* the reaction of $^{\cdot}O_2^-$ and Fe (II) (Eq. (3)). The higher RhB degradation depression efficiency caused by SOD than CAT suggested that the sequential single-electron transfer route ($O_2 \rightarrow {}^{\cdot}O_2^- \rightarrow H_2O_2 \rightarrow {}^{\cdot}OH$) was the major pathway of $^{\cdot}OH$ generation in the Fe@Fe_2O_3/PCA system.

$$2{\cdot}O_2^- + 2H_2O \xrightarrow{SOD} H_2O_2 + O_2 + 2OH^- \quad (2)$$

$${\cdot}O_2^- + 2H^+ + Fe(II) \rightarrow H_2O_2 + Fe(III) \quad (3)$$

As well-known, EDTA is popular complexing agent which could stabilize the dissolved Fe species. PCA can not only act as complexing agent to accelerate the leaching/dissolution Fe species and stabilize the dissolved Fe(III), but also enhance the Fe(III)/Fe(II) cycle in the system. Therefore, the RhB degradation efficiency in the Fe@Fe_2O_3/PCA and Fe@Fe_2O_3/EDTA systems were investigated systematically at different pH value. For the acidic nature of PCA and EDTA, the initial pH values of the Fe@Fe_2O_3/PCA and Fe@Fe_2O_3/EDTA systems without pH adjustment were 3.9 and 3.5 respectively. As shown in Fig. S4A in the Supporting information, the degradation efficiency of RhB in the system

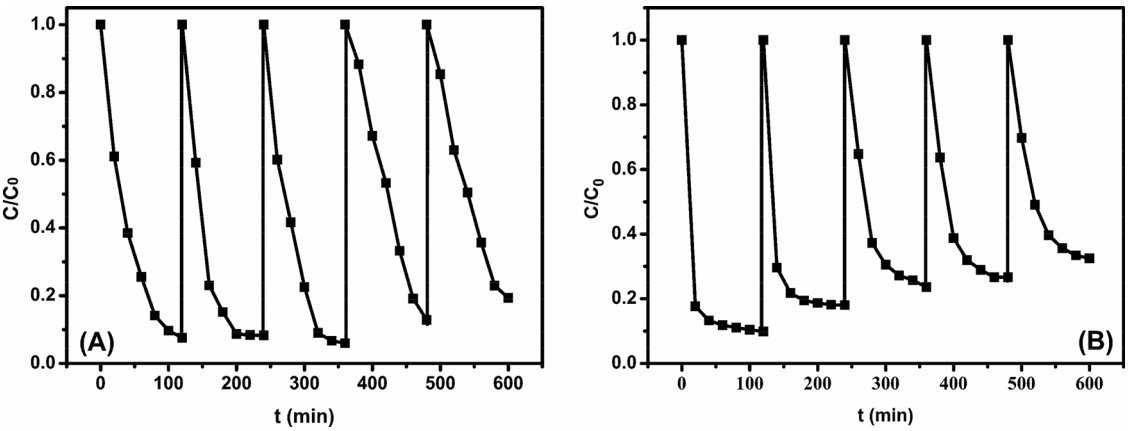

Fig. 4. Recycling experiments of $Fe@Fe_2O_3$ foraerobic RhB degradation in (A) $Fe@Fe_2O_3$/PCA and (B) $Fe@Fe_2O_3$/EDTA systems. The initial concentrations of RhB, $Fe@Fe_2O_3$, PCA, and EDTA were 5 mg L^{-1}, 4.5, 0.5 and 0.5 mmol L^{-1}, respectively.

with PCA and EDTA decreased from 92.4% to 11.1% and 90.1% to 81.0% within 120 min when the initial pH value increased to 7 (Fig. S4B in the Supporting information). This is because PCA can only function as the complexing and reducing agent to maintain iron in soluble forms and quickly reduce Fe(III) to Fe(II) at acidic pH. After the reaction, $Fe@Fe_2O_3$ was found to be still black in the presence of PCA, while it was changed to red brown when EDTA was added. So, the reusability of $Fe@Fe_2O_3$ core-shell nanowires in the system were also compared with PCA and EDTA. The degradation rate of RhB in the $Fe@Fe_2O_3$/PCA system was appreciably lower than that of the $Fe@Fe_2O_3$/EDTA system, but $Fe@Fe_2O_3$ core-shell nanowires in the system with PCA presented good reusability (Fig. 4). No significantly decrease of RhB degradation efficiency was observed after 3 cycles in the system with PCA. The degradation efficiency of RhB reached 80.7% after 5 cycles in the presence of PCA. However, only 76.4% and 67.5% of RhB was degraded after 3 and 5 cycles with the addition of EDTA, respectively. This significant difference may be attributed to two factors. One was that the complexing ability of PCA was much weaker than that of the EDTA, resulting in the lower corrosion rate of $Fe@Fe_2O_3$ core-shell nanowires [36,42]. The other was explained that PCA could be degraded along with organic contaminants, leading to the decrease of iron ions concentrations.

Then, scanning electron microscopy (SEM) and X-ray diffraction (XRD) analysis were used to probe the morphology and phase changes of $Fe@Fe_2O_3$ core-shell nanowires before and after the first time of aerobic RhB degradation in the system of PCA or EDTA. The as-prepared $Fe@Fe_2O_3$ core-shell nanowires were of abundant necklace-like nanowires with 50–100 nm in diameter and several tens of micrometers in length (Fig. S5A in the Supporting information). However, the wire-like shape of $Fe@Fe_2O_3$ core-shell nanowires were destroyed and agglomerated into irregular nanoparticles and some plate-like nanoparticles for the deposition of corrosion products after the aerobic RhB degradation in the presence of PCA or EDTA (Fig. S5B, C in the Supporting information). The agglomeration of $Fe@Fe_2O_3$ core-shell nanowires in the system with EDTA was much more serious than the system with PCA. The diameters of the nanoparticles in the system with PCA were several hundreds of nanometers, while the $Fe@Fe_2O_3$ core-shell nanowires aggregated in clumps in the system with EDTA. An obvious diffraction peak at 2θ value of 44.9°, which can be assigned to the standard pattern of Fe (JCPDS, file no. 3-1050), was detected in the as-prepared $Fe@Fe_2O_3$ core-shell nanowires (Fig. 5A). The diffraction peak of Fe_2O_3 could not be detected because the amorphous nature of Fe_2O_3 or the thickness of the Fe_2O_3 shell is too small, which was consistent with our previous work [43]. No apparent changes were observed in the XRD pattern of $Fe@Fe_2O_3$ core-shell nanowires after the aerobic RhB degradation in the system with PCA, while some new diffraction peaks appeared in the presence of EDTA. The new peaks

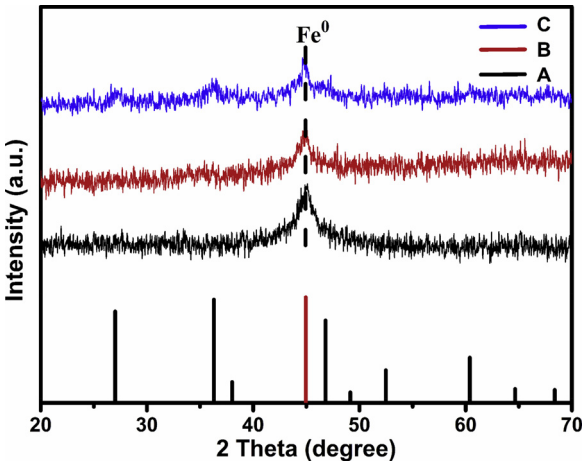

Fig. 5. XRD patterns of $Fe@Fe_2O_3$ core-shell nanowires. (A) Before the reaction. After aerobic RhB degradation in (B) $Fe@Fe_2O_3$/PCA and (C) $Fe@Fe_2O_3$/EDTA systems.

matched well with the standard pattern of FeOOH (JCPDS, file no. 1-136), a corrosion product of the Fe^0 (Fig. 5B). These results suggested that the oxidation degree and the thickness of oxide layer would be the main factors affecting the reactivity of $Fe@Fe_2O_3$ core-shell nanowires rather than its morphology. The oxide layer of $Fe@Fe_2O_3$ core-shell nanowires in the system with PCA was much thinner than the system with EDTA. The increase of iron oxide thickness would block the outward electron transfer from iron core and thus inhibit the subsequent molecular oxygen activation. So, the RhB degradation efficiency in the $Fe@Fe_2O_3$/EDTA system decreased as the reused cycle number increased.

Besides the thickness of iron oxide, surface bound ferrous ions on the iron oxide shell was also an important factor affecting the reactivity of $Fe@Fe_2O_3$ core-shell nanowires. Therefore, the $Fe@Fe_2O_3$ core-shell nanowires before and after the first time of aerobic RhB degradation in the presence of PCA or EDTA was also further analyzed using X-ray photoelectron spectroscopy (XPS) to investigate the surface chemical compositions. The photoelectron peaks revealed that the as-prepared $Fe@Fe_2O_3$ core-shell nanowires is composed of two elements, Fe and O. No other C 1s peak but the adventitious carbon could be observed in the high resolution in the as-prepared $Fe@Fe_2O_3$ (Fig. S6 in the Supporting information). However, the C 1s spectrum or C 1s and N 1s spectra were easily observed in the used $Fe@Fe_2O_3$ with PCA or EDTA, respectively. The high-resolution C 1 s peaks at 286, 288 and 290.2 eV, which are assigned to the C—OH, C═O, and O═C—OH, respectively (Fig. 6A). The high-resolution N1 s peak of the used $Fe@Fe_2O_3$ with EDTA could

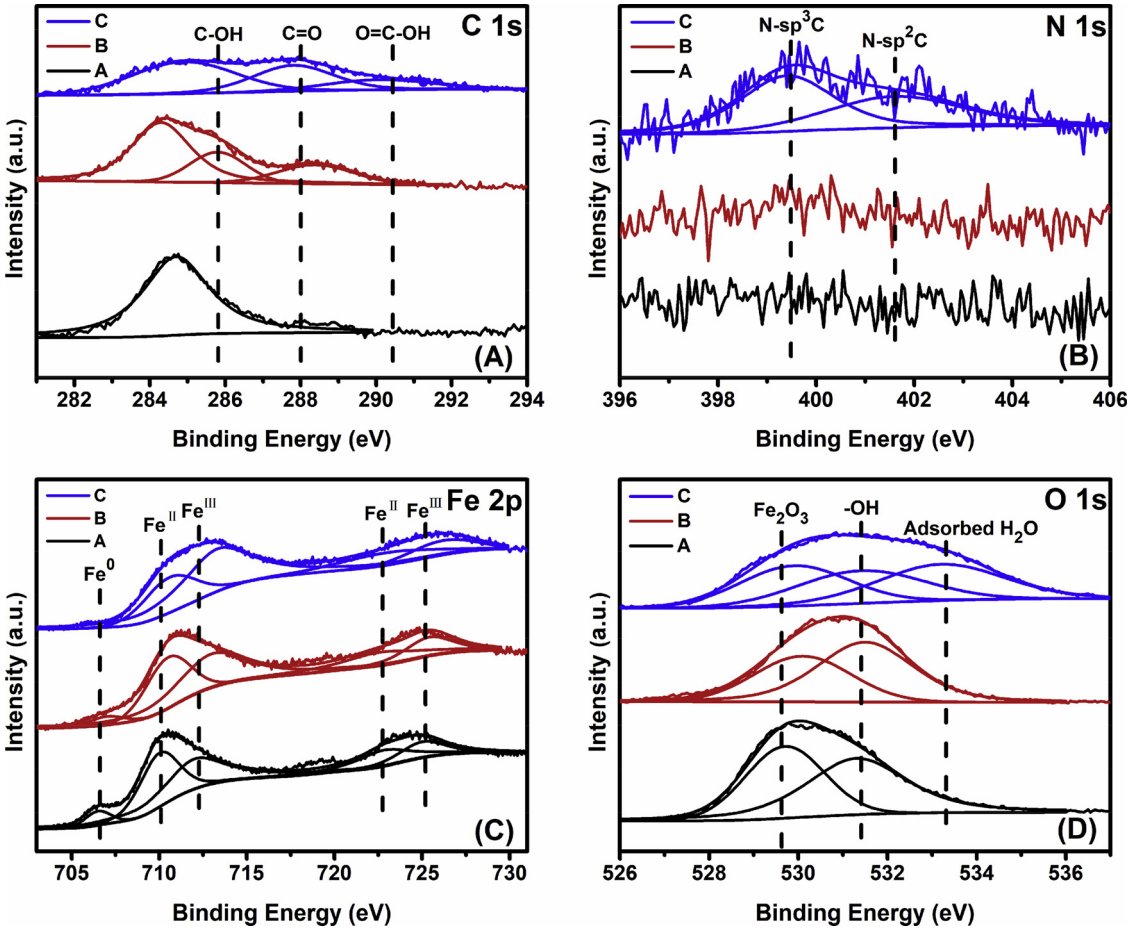

Fig. 6. High resolution spectra of (A) C 1s, (B) N 1s, (C) Fe 2p, and (D) O 1s within XPS spectra of Fe@Fe_2O_3 core-shell nanowires.

Table 1
Molar ratios of Fe^0/Fe_{total}, Fe^{II}/Fe_{total}, and Fe^{III}/Fe_{total} in Fe 2p spectra and O_{Fe2O3}/O_{total} and O_{OH}/O_{total} in O 1s of Fe@Fe_2O_3 core-shell nanowires. (A) Before the reaction. After aerobic RhB degradation in (B) Fe@Fe_2O_3/PCA and (C) Fe@Fe_2O_3/EDTA systems.

Samples	Fe^0/Fe_{total}	Fe^{II}/Fe_{total}	Fe^{III}/Fe_{total}	$O_{Fe_2O_3}/O_{total}$	O_{OH}/O_{total}	O_{H_2O}/O_{total}
A	0.048	0.464	0.488	0.441	0.559	—
B	0.036	0.456	0.508	0.500	0.500	—
C	—	0.371	0.629	0.324	0.310	0.366

be fitted by two peaks at the binding energies of 399.4 and 400.9 eV (Fig. 6B), which assigned to the N-sp^3C, and N-sp^2C, respectively. These results suggested the adsorption or the complex of RhB and its degradation products, PCA, and EDTA on the surface of the used Fe@Fe_2O_3. The high-resolution spectra of N 1 s could not be detected in the used Fe@Fe_2O_3 with PCA due to the low content of nitrogen element. Photoelectron peaks of the Fe 2p region at 706.7 eV suggested the existence of zerovalent iron (Fe^0) in the as-prepared and used Fe@Fe_2O_3 with PCA (Fig. 6C). The peak of Fe° disappeared after the aerobic RhB degradation in the system with EDTA, which was consistent with the SEM and XRD results. Meanwhile, the ratio of ferrous iron to total iron (Fe^{II}/Fe_{total}) and ferric iron to total iron (Fe^{III}/Fe_{total}) were also calculated from the peak areas in the Fe 2p spectra (Table 1). It was found that Fe^{II}/Fe_{total} and Fe^{III}/Fe_{total} of the used Fe@Fe_2O_3 core-shell nanowires with PCA changed slightly from 0.464 and 0.488 to 0.456 and 0.508, respectively. However, the Fe^{II}/Fe_{total} of the used Fe@Fe_2O_3 with EDTA decreased from 0.464 to 0.371, while Fe^{III}/Fe_{total} increased from 0.488 to 0.629. In addition, the O 1 s spectrum could be fitted very well with peaks at 529.7, 531.3 eV, and 533.2 eV (Fig. 6D), which are the characteristics of lattice oxygen binding with Fe (Fe_2O_3) and oxygen in hydroxyl groups (−OH) and adsorbed water (H_2O), respectively. The ratio of oxygen in oxides to total oxygen (O_{Fe2O3}/O_{total}) in Fe@Fe_2O_3 core-shell nanowires increased in from 0.441 to 0.50 after the aerobic RhB degradation with PCA (Table 1). Although the adsorbed water leaded to the decrease of the O_{Fe2O3}/O_{total} in the used Fe@Fe_2O_3 with EDTA, the ratio of oxygen in oxides to hydroxyl groups (O_{Fe2O3}/O_{OH}) in the used Fe@Fe_2O_3 with EDTA was significantly higher than PCA. These results further confirm the formation of more iron oxides in the system with EDTA.

Total organic carbon (TOC) analysis was then employed to probe the fates of RhB, PCA, and EDTA in both of the Fe@Fe_2O_3/PCA and Fe@Fe_2O_3/EDTA systems. As all of RhB, PCA, and EDTA contributed to the TOC values, the TOC changes of the two systems were compared in the presence or absence of RhB. Obviously, the TOC changes in the absence of RhB reflected the mineralization of PCA or EDTA, and the TOC removal of RhB could be calculated by the differences of TOC in the presence or absence of RhB. The initial TOC values of the Fe@Fe_2O_3/PCA systems in the presence or absence of RhB were obtained as 41.0 and 37.7 mg L^{-1}, while initial TOC values of the Fe@Fe_2O_3/EDTA systems in the presence or absence of RhB were obtained as 58.3 and 55.1 mg L^{-1} (Fig. 7). Therefore, the initial TOC values of RhB in the Fe@Fe_2O_3/PCA and Fe@Fe_2O_3/EDTA systems were calculated to be 3.3 and 3.2 mg L^{-1}, respectively, which were consistent with the theoretical value (3.5 mg L^{-1}). As shown in Fig. 7, 71.3% of PCA and 16.1% of RhB was mineralized within 120 min in the Fe@Fe_2O_3/PCA system, but only slightly mineralization of EDTA (7.6%) was detected in the Fe@Fe_2O_3/EDTA system. Therefore, the Fe@Fe_2O_3/PCA system exhibited lower RhB degradation rate but higher TOC removal efficiency than the

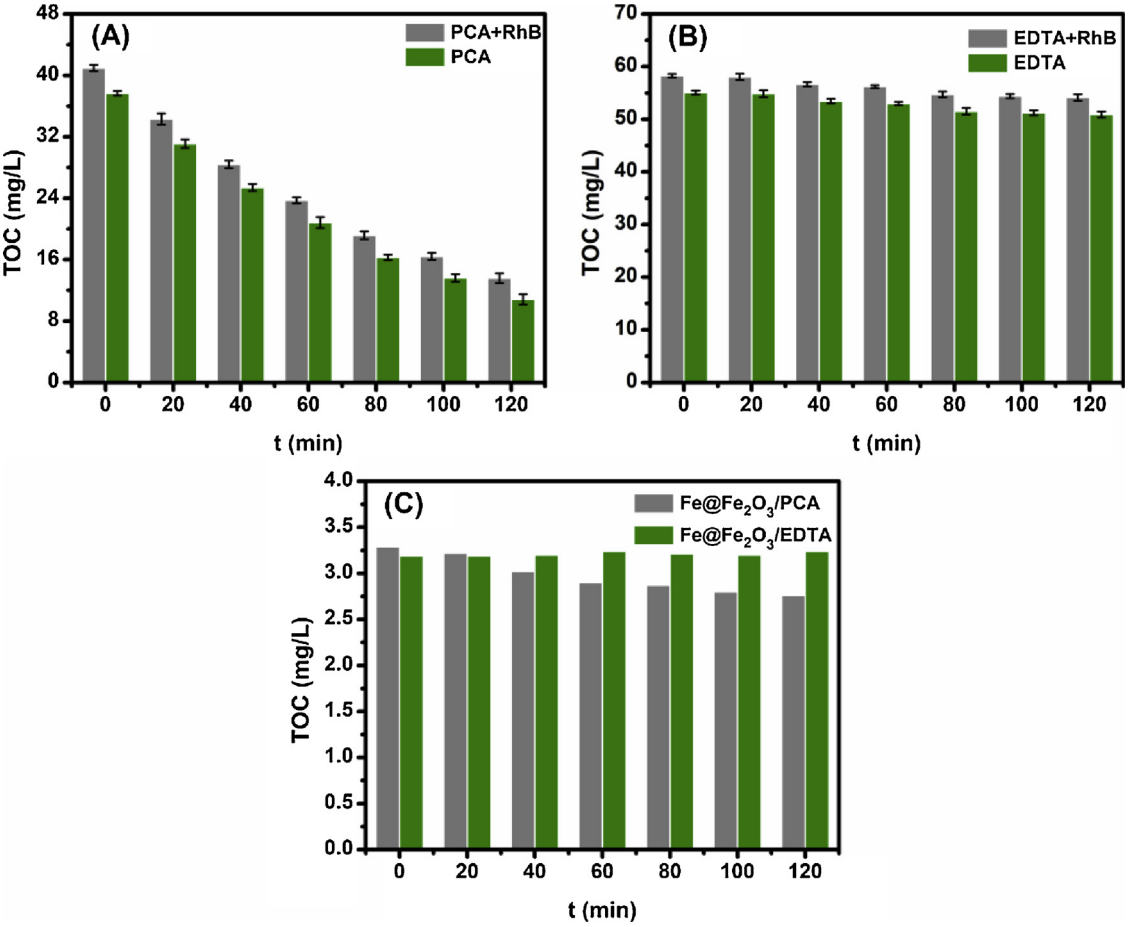

Fig. 7. Time profiles of TOC removal in the (A) $Fe@Fe_2O_3$/PCA and (B) $Fe@Fe_2O_3$/EDTA systems in the presence and absence of RhB. (C) TOC changes of RhB in the in the $Fe@Fe_2O_3$/PCA system and $Fe@Fe_2O_3$/EDTA systems. The initial concentrations of RhB, $Fe@Fe_2O_3$, PCA, and EDTA were 5 mg L^{-1}, 4.5, 0.5 and 0.5 mmol L^{-1}, respectively.

$Fe@Fe_2O_3$/EDTA system. To clarify these differences, the degradation rate constants of ligands and $^{\cdot}OH$ as well as the degradation mechanisms of RhB were compared in the two systems. The reaction rate constant for $^{\cdot}OH$ with PCA (5×10^9 $M^{-1}{\cdot}s^{-1}$) is higher than that of EDTA, resulting in the faster mineralization rate of PCA during the simultaneous RhB and ligands removal processes. Then, the UV–vis spectra indicated the different degradation mechanisms of RhB in the two systems (Fig. S7 in the Supporting information). A new peak appeared at 600–700 nm was attributed to the complexes of Fe(III)-PCA. The characteristic absorption band of RhB at 554 nm decreased along with the increase of reaction time in the $Fe@Fe_2O_3$/PCA system, suggesting the cleavage of the conjugated xanthene ring in RhB [44]. While a significant blue shift was observed in the $Fe@Fe_2O_3$/EDTA system, which was due to an N-dealkylation process of RhB [45,46].

4. Conclusions

Molecular oxygen activation with ZVI is a promising technology for wastewater treatment and groundwater remediation due to their simplicity, environmental friendliness, and ubiquitous existence in natural environment. Unfortunately, the low yield of RS extremely restricted its practical application. The addition of EDTA can not only promoted the yield of RS, but also accelerate the oxidation of ZVI. In this study, PCA, a kind of phenolic acid, which was found widely existed in many plants, could effectively promote the catalyzed activation efficiency of molecular oxygen with $Fe@Fe_2O_3$ core-shell nanowires. Although the degradation rate of RhB in the system with PCA was lower than the system with EDAT during the first cycle, no obvious decrease in the activity of $Fe@Fe_2O_3$ core-shell nanowires was observed in the degradation efficiencies of RhB with PCA after three cycles. Moreover, PCA can not only promoted the degradation and mineralization of RhB with $Fe@Fe_2O_3$ core-shell nanowires, but also mineralized along with RhB, which can further reduce the environmental risk caused by the residual aminopoly (carboxylic acid) chelators. As well-known, both PCA and ZVI are ubiquitous in natural environments. Understanding the promotion effect on molecular activation mechanism of ZVI with PCA will be helpful in the practical applications of ZVI in environment remediation.

Acknowledgements

This work was financially supported by National Natural Science Funds for Distinguished Young Scholars (41425015 and 21425728), National Natural Science Foundation of China (41573086), Leading Scientific, Technical and Innovation Talents of Guangdong special support program (2016TX03Z094), and China Postdoctoral Science Foundation (2017M612609).

Appendix A. Supplementary data

Supplementary material related to this article can be found, in the online version, at doi:https://doi.org/10.1016/j.cattod.2018.10.058.

References

[1] Y.X. Qin, G.Y. Li, Y.P. Gao, L.Z. Zhang, Y.S. Ok, T.C. An, Persistent free radicals in carbon-based materials on transformation of refractory organic contaminants

(ROCs) in water: a critical review, Water Res. 137 (2018) 130–143.
[2] R. Mukherjee, R. Kumar, A. Sinha, Y. Lama, A.K. Saha, A review on synthesis, characterization, and applications of nano zero valent iron (nZVI) for environmental remediation, Crit. Rev. Environ. Sci. Technol. 46 (2015) 443–466.
[3] G.Y. Li, X. Nie, J.Y. Chen, Q. Jiang, T.C. An, P.K. Wong, H.M. Zhang, H.J. Zhao, H. Yamashita, Enhanced visible-light-driven photocatalytic inactivation of Escherichia coli using g-C_3N_4/TiO_2 hybrid photocatalyst synthesized using a hydrothermal-calcination approach, Water Res. 86 (2015) 17–24.
[4] F. Fu, D.D. Dionysiou, H. Liu, The use of zero-valent iron for groundwater remediation and wastewater treatment: a review, J. Hazard. Mater. 267 (2014) 194–205.
[5] Y. Sun, J. Li, T. Huang, X. Guan, The influences of iron characteristics, operating conditions and solution chemistry on contaminants removal by zero-valent iron: a review, Water Res. 100 (2016) 277–295.
[6] Y.D. Zou, X.X. Wang, A. Khan, P.Y. Wang, Y.H. Liu, A. Alsaedi, T. Hayat, X.K. Wang, Environmental remediation and application of nanoscale zero-valent iron and its composites for the removal of heavy metal ions: a review, Environ. Sci. Technol. 50 (2016) 7290–7304.
[7] S.-H. Kang, A.D. Bokare, Y. Park, C.H. Choi, W. Choi, Electron shuttling catalytic effect of mellitic acid in zero-valent iron induced oxidative degradation, Catal. Today 282 (2017) 65–70.
[8] S.M. Ponder, J.G. Darab, T.E. Mallouk, Remediation of Cr(VI) and Pb(II) aqueous solutions using supported, nanoscale zero-valent iron, Environ. Sci. Technol. 34 (2000) 2564–2569.
[9] L.N. Shi, X. Zhang, Z.L. Chen, Removal of chromium (VI) from wastewater using bentonite-supported nanoscale zero-valent iron, Water Res. 45 (2011) 886–892.
[10] M.H. Liu, Y.H. Wang, L.T. Chen, Y. Zhang, Z. Lin, $Mg(OH)_2$ supported nanoscale zero valent iron enhancing the removal of Pb(II) from aqueous solution, ACS Appl. Mater. Interfaces 7 (2015) 7961–7969.
[11] T.Y. Liu, Z.L. Wang, L. Zhao, X. Yang, Enhanced chitosan/Fe°-nanoparticles beads for hexavalent chromium removal from wastewater, Chem. Eng. J. 189–190 (2012) 196–202.
[12] A. Ryu, S.W. Jeong, A. Jang, H. Choi, Reduction of highly concentrated nitrate using nanoscale zero-valent iron: effects of aggregation and catalyst on reactivity, Appl. Catal. B: Environ. 105 (2011) 128–135.
[13] Y.H. Hwang, D.G. Kim, H.S. Shin, Mechanism study of nitrate reduction by nano zero valent iron, J. Hazard. Mater. 185 (2011) 1513–1521.
[14] S.H. Joo, A.J. Feitz, T.D. Waite, Oxidative degradation of the carbothioate herbicide, molinate, using nanoscale zero-valent iron, Environ. Sci. Technol. 38 (2004) 2242–2247.
[15] S. Chen, J. Bedia, H. Li, L.Y. Ren, F. Naluswata, C. Belver, Nanoscale zero-valent iron@mesoporous hydrated silica core-shell particles with enhanced dispersibility, transportability and degradation of chlorinated aliphatic hydrocarbons, Chem. Eng. J. 343 (2018) 619–628.
[16] D.H. Bremner, A.E. Burgess, D. Houllemare, K.-C. Namkung, Phenol degradation using hydroxyl radicals generated from zero-valent iron and hydrogen peroxide, Appl. Catal. B: Environ. 63 (2006) 15–19.
[17] R. Ling, J.P. Chen, J. Shao, M. Reinhard, Degradation of organic compounds during the corrosion of ZVI by hydrogen peroxide at neutral pH: kinetics, mechanisms and effect of corrosion promoting and inhibiting ions, Water Res. 134 (2018) 44–53.
[18] S.A. Messele, O.S.G.P. Soares, J.J.M. Órfão, C. Bengoa, F. Stüber, A. Fortuny, A. Fabregat, J. Font, Effect of activated carbon surface chemistry on the activity of ZVI/AC catalysts for Fenton-like oxidation of phenol, Catal. Today 240 (2015) 73–79.
[19] A. Ziylan, N.H. Ince, Catalytic ozonation of ibuprofen with ultrasound and Fe-based catalysts, Catal. Today 240 (2015) 2–8.
[20] C. Kim, J.Y. Ahn, T.Y. Kim, W.S. Shin, I. Hwang, Activation of persulfate by nanosized zero-valent iron (NZVI): mechanisms and transformation products of NZVI, Environ. Sci. Technol. 52 (2018) 3625–3633.
[21] M.A. Al-Shamsi, N.R. Thomson, Treatment of organic compounds by activated persulfate ssing nanoscale zerovalent iron, Ind. Eng. Chem. Res. 52 (2013) 13564–13571.
[22] C.J. Liang, Y.Y. Guo, Mass transfer and chemical oxidation of naphthalene particles with zerovalent iron activated persulfate, Environ. Sci. Technol. 44 (2010) 8203–8208.
[23] J. Xu, X. Wang, F. Pan, Y. Qin, J. Xia, J. Li, F. Wu, Synthesis of the mesoporous carbon-nano-zero-valent iron composite and activation of sulfite for removal of organic pollutants, Chem. Eng. J. 353 (2018) 542–549.
[24] S.Y. Pang, J. Jiang, J. Ma, Oxidation of sulfoxides and arsenic(III) in corrosion of nanoscale zero valent iron by oxygen: evidence against ferryl Ions (Fe(IV)) as active intermediates in Fenton reaction, Environ. Sci. Technol. 45 (2011) 307–312.
[25] J.X. Li, X.Y. Zhang, M.C. Liu, B.C. Pan, W.M. Zhang, Z. Shi, X.H. Guan, Enhanced reactivity and electron selectivity of sulfidated zerovalent iron toward chromate under aerobic conditions, Environ. Sci. Technol. 52 (2018) 2988–2997.
[26] J.X. Li, X.Y. Zhang, Y.K. Sun, L.P. Liang, B.C. Pan, W.M. Zhang, X.H. Guan, Advances in sulfidation of zerovalent iron for water decontamination, Environ. Sci. Technol. 51 (2017) 13533–13544.
[27] X. Huang, X. Hou, F. Jia, F. Song, J. Zhao, L. Zhang, Ascorbate-promoted surface iron cycle for efficient heterogeneous Fenton alachlor degradation with hematite nanocrystals, ACS Appl. Mater. Interfaces 9 (2017) 8751–8758.
[28] X. Huang, X. Hou, X. Zhang, K.M. Rosso, L. Zhang, Facet-dependent contaminant removal properties of hematite nanocrystals and their environmental implications, Environ. Sci. Nano 5 (2018) 1790–1806.
[29] X. Huang, X. Hou, J. Zhao, L. Zhang, Hematite facet confined ferrous ions as high efficient Fenton catalysts to degrade organic contaminants by lowering H_2O_2 decomposition energetic span, Appl. Catal. B: Environ. 181 (2016) 127–137.
[30] S.H. Joo, A.J. Feitz, D.L. Sedlak, T.D. Waite, Quantification of the oxidizing capacity of nanoparticulate zero-valent iron, Environ. Sci. Technol. 39 (2005) 1263–1268.
[31] L. Wang, M.H. Cao, Z.H. Ai, L.Z. Zhang, Dramatically enhanced aerobic atrazine degradation with Fe@Fe_2O_3 core-shell nanowires by tetrapolyphosphate, Environ. Sci. Technol. 48 (2014) 3354–3362.
[32] C.H. Xu, B.H. Zhang, Y.L. Wang, Q.Q. Shao, W.Z. Zhou, D.M. Fan, J.Z. Bandstra, Z.Q. Shi, P.G. Tratnyek, Effects of sulfidation, magnetization, and oxygenation on azo dye reduction by zerovalent iron, Environ. Sci. Technol. 50 (2016) 11879–11887.
[33] X. Hou, X. Huang, Z. Ai, J. Zhao, L. Zhang, Ascorbic acid/Fe@Fe_2O_3: a highly efficient combined Fenton reagent to remove organic contaminants, J. Hazard. Mater. 310 (2016) 170–178.
[34] X. Hou, X. Huang, F. Jia, Z. Ai, J. Zhao, L. Zhang, Hydroxylamine promoted goethite surface Fenton degradation of organic pollutants, Environ. Sci. Technol. 51 (2017) 5118–5126.
[35] X. Hou, X. Huang, M. Li, Y. Zhang, S. Yuan, Z. Ai, J. Zhao, L. Zhang, Fenton oxidation of organic contaminants with aquifer sediment activated by ascorbic acid, Chem. Eng. J. 348 (2018) 255–262.
[36] C.R. Keenan, D.L. Sedlak, Ligand-enhanced reactive oxidant generation by nanoparticulate zero-valent iron and oxygen, Environ. Sci. Technol. 42 (2008) 6936–6941.
[37] Q. Huang, M.H. Cao, Z.H. Ai, L.Z. Zhang, Reactive oxygen species dependent degradation pathway of 4-chlorophenol with Fe@Fe_2 O_3 core–shell nanowires, Appl. Catal. B: Environ. 162 (2015) 319–326.
[38] L.R. Lu, Z.H. Ai, J.P. Li, Z. Zheng, Q. Li, Lz. Zhang, Synthesis and characterization of Fe-Fe_2O_3 core-shell nanowires and nanonecklaces, Cryst. Growth Des. 7 (2007) 459–464.
[39] L. Wang, F. Wang, P.N. Li, L.Z. Zhang, Ferrous-tetrapolyphosphate complex induced dioxygen activation for toxic organic pollutants degradation, Sep. Purif. Technol. 120 (2013) 148–155.
[40] W. Liu, Z.H. Ai, M.H. Cao, L.Z. Zhang, Ferrous ions promoted aerobic simazine degradation with Fe@Fe_2O_3 core–shell nanowires, Appl. Catal. B: Environ. 150–151 (2014) 1–11.
[41] G.D. Fang, C. Liu, J. Gao, D.M. Zhou, New insights into the mechanism of the catalytic decomposition of hydrogen peroxide by activated carbon: implications for degradation of diethyl phthalate, Ind. Eng. Chem. Res. 53 (2014) 19925–19933.
[42] C.E. Noradoun, I.F. Cheng, EDTA degradation induced by oxygen activation in a zerovalent iron/air/water system, Environ. Sci. Technol. 39 (2005) 7158–7163.
[43] Z.H. Ai, Z.T. Gao, L.Z. Zhang, W.W. He, J.J. Yin, Core-shell structure dependent reactivity of Fe@Fe_2O_3 nanowires on aerobic degradation of 4-chlorophenol, Environ. Sci. Technol. 47 (2013) 5344–5352.
[44] Z.H. Wang, W.H. Ma, C.C. Chen, J.C. Zhao, Light-assisted decomposition of dyes over iron-bearing soil clays in the presence of H_2O_2, J. Hazard. Mater. 168 (2009) 1246–1252.
[45] H.B. Fu, S.C. Zhang, T.G. Xu, Y.F. Zhu, J.M. Chen, Photocatalytic degradation of RhB by fluorinated Bi_2WO_6 and distributions of the intermediate products, Environ. Sci. Technol. 42 (2008) 2085–2091.
[46] J.D. Zhuang, W.X. Dai, Q.F. Tian, Z.H. Li, L.Y. Xie, J.X. Wang, P. Liu, X.C. Shi, D.H. Wang, Photocatalytic degradation of RhB over TiO_2 bilayer films: effect of defects and their location, Langmuir 26 (2010) 9686–9694.